Experimental and numerical assessment of low-frequency current distributions from UMTS and GSM mobile phones

2013 Phys. Med. Biol. 58 8339

(http://iopscience.iop.org/0031-9155/58/23/8339)

IOP Publishing Physics in Medicine and Biology

Phys. Med. Biol. **58** (2013) 8339–8357 doi:10.1088/0031-9155/58/23/8339

Experimental and numerical assessment of low-frequency current distributions from UMTS and GSM mobile phones

Marie-Christine Gosselin[1,2], **Sven Kühn**[1,2] **and Niels Kuster**[1,2]

[1] Foundation for Research on Information Technologies in Society (IT'IS), Zeughausstrasse 43, 8004 Zurich, Switzerland
[2] ETH Zurich, Zurich, Switzerland

E-mail: gosselin@itis.ethz.ch

Received 15 July 2013, in final form 11 October 2013
Published 11 November 2013
Online at stacks.iop.org/PMB/58/8339

Abstract

The evaluation of the exposure from mobile communication devices requires consideration of electromagnetic fields (EMFs) over a broad frequency range from dc to GHz. Mobile phones in operation have prominent spectral components in the low-frequency (LF) and radio-frequency (RF) ranges. While the exposure to RF fields from mobile phones has been comprehensively assessed in the past, the LF fields have received much less attention. In this study, LF fields from mobile phones are assessed experimentally and numerically for the global system for mobile (GSM) and universal mobile telecommunications system (UMTS) communication systems and conclusions about the global (LF and RF) EMF exposure from both systems are drawn. From the measurements of the time-domain magnetic fields, it was found that the contribution from the audio signal at a normal speech level, i.e., −16 dBm0, is the same order of magnitude as the fields induced by the current bursts generated from the implementation of the GSM communication system at maximum RF output level. The *B*-field induced by currents in phones using the UMTS is two orders of magnitude lower than that induced by GSM. Knowing that the RF exposure from the UMTS is also two orders of magnitude lower than from GSM, it is now possible to state that there is an overall reduction of the exposure from this communication system.

(Some figures may appear in colour only in the online journal)

1. Introduction

Over the past two decades, numerous scientists have investigated the possible effects of electromagnetic fields (EMFs) on humans. Studies have been conducted to identify potential biological effects due to exposure to weak EMF over a broad frequency range covering extremely low frequencies to radio frequencies. Although there are various findings of

biological effects reported in the low-frequency (LF) and radio-frequency (RF) ranges, a concrete mechanism has not yet been established. Thus, the effects from any particular frequency range cannot be disregarded when assessing the exposure to complex transmitters such as mobile phones, which generate fields in various frequency ranges (LF and RF).

Currently, mobile phones operated at the human head are considered the strongest source of human exposure to RF EMF, i.e., worst-case exposure can approach the established safety limits. Over the past decade, the majority of exposure assessment studies have focused on exposure to the strong RF EMF generated by phone antennas operating at frequencies between 400 MHz and 3 GHz. However, LF EMF, i.e., lower than 20 kHz, are also generated by other elements of the phone, e.g., by the supply currents or the audio speaker. There are considerably fewer studies that address the characterization of exposure to these fields from mobile phones used in the normal operating mode, i.e., at the head.

While there is a very limited number of studies that have assessed LF exposure from mobile phones using global system for mobile (GSM) communications experimentally (Andersen and Pedersen 1997, Jokela *et al* 2004, Perentos *et al* 2007, Tuor *et al* 2005) and numerically (Ilvonen *et al* 2005, Ilvonen and Sarvas 2007, Perentos *et al* 2008), there is no data at all in the literature on LF exposure from phones using the universal mobile telecommunications system (UMTS) communication system. Despite this, UMTS technologies are becoming more and more common as GSM technology is slowly being phased out. Characterization of the RF output power of UMTS phones has shown that the average exposure to RF EMF of this communication system is smaller than that of GSM by more than a factor of 100 (Kuehn and Kuster 2013). Nevertheless, a recommendation for this technology cannot be made until evaluation of the LF exposure, which has the potential to be higher than that of GSM due to the higher current consumption of UMTS[3] signal processors, has been completed.

The objective of this study is to close the gap in the knowledge of the LF exposure from mobile phones using GSM and UMTS networks. In detail, that includes:

- experimental assessment of the *B*-fields from mobile phones in GSM900, GSM1800, and UMTS1950 bands, and
- evaluation of the compliance with safety guidelines/standards based on induced fields and current density in anatomical heads.

2. Methods

2.1. Communication systems

Communication channel separation in GSM (3GPP 1999) is implemented with time division multiple access (TDMA), which results in transmission bursts. Dominant supply currents are drawn in bursts with frequency components at 217 (frame frequency) and 8.3 Hz (1/26 missing frame). Wideband code division multiple access (W-CDMA) (3GPP 2002) is used to separate the communication channels in UMTS. Since the transmission with the base station is quasi-continuous, the current from the battery is not drawn in bursts. Both communication systems might exhibit additional weak LF spectral components due to power control contributions at <2 Hz for GSM (Wiart *et al* 2000) as well as 750 and 1500 Hz for UMTS (Pedersen and Andersen 1999, Andersen *et al* 2010).

[3] Here, the term UMTS is used to refer to UMTS-FDD, which is more frequently employed than UMTS-TDD, mainly used for data transfer.

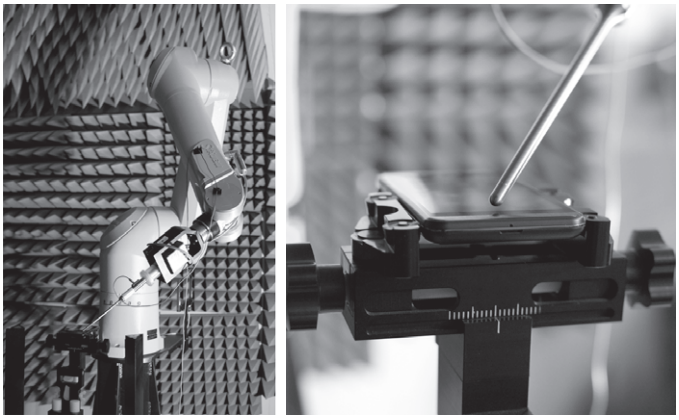

Figure 1. Left: DASY52 NEO scanner with *B*-field probe. Right: LF *B*-field probe at a distance of 1 mm from the mobile phone surface (LG Optimum 3D P920).

Table 1. Measurement equipment specifications.

Description	Specification
Positioner system	SPEAG DASY52 NEO
Repeatability	±0.2 mm
Magnetic field measurement system	
Probe	SPEAG AM1DV3
Sensor-to-surface distance	3 mm
Sensitivity	<0.1nT at 1 kHz
Dynamic range	−100 dB
Frequency range	60 Hz–20 kHz
Signal and sampling unit	SPEAG AMMI
Sampling rate	48 kHz (iTDMAn and out)
Radio communication tester	Rohde and Schwarz CMU200

2.2. Experimental setup

2.2.1. Equipment. The measurements were performed with the dosimetric assessment system DASY 52 NEO (Schmid and Partners Engineering AG, SPEAG, Switzerland) (table 1). The small probe size of this system allows measurements to be performed very close to the phones' surfaces (see figure 1), which was not possible with the large probes used in previous studies (Perentos *et al* 2007, Tuor *et al* 2005). The Python interface implemented in the DASY 52 NEO software allowed flexible integration of the time-domain measurements into the software. The communication link from the phone was established and controlled with a radio communication tester (Rohde and Schwarz CMU200).

2.2.2. Exposure scenarios. Table 2 shows the main characteristics of the ten selected devices under test (DUTs). The measurement planes were defined as parallel to the surface at a distance of 1 mm from the probe tip at the highest phone location, leading to a minimum distance of 4 mm between the sensor and the phone surface.

Area scans were performed with a resolution of $5 \times 7\,\mathrm{mm}^2$ over the entire area of the phone. A higher-resolution scan ($3 \times 3\,\mathrm{mm}^2$) was performed around the audio output with the

Table 2. Main characteristics of the DUTs.

ID	Phone model	Type	OS	Release date
Nokia 6120	Nokia 6120	Bar	-	April 2007
Sony Ericsson W910	Sony Ericsson W910i	Slide	-	Oct 2007
Sony Ericsson W760i	Sony Ericsson W760i	Slide	-	May 2008
MotorolaV1050	Motorola V1050	Flip	-	January 2005
HTCdiam100	HTC Diam100 Touch Diamond	Smart	Windows phone	May 2008
HTCtopa100	HTC Topa100 Touch Diamond2	Smart	Windows phone	April 2009
iPhone3 g	Apple iPhone 3 g	Smart	iOS	July 2008
iPhone4	Apple iPhone 4	Smart	iOS	June 2010
SamsungGT-I9001	Samsung Galaxy GT-I9001	Smart	Android	June 2010
LG	LG P920 Optimus 3D	Smart	Android	July 2011

Table 3. PCL and corresponding typical average RF power for each communication system.

	0 dB		−6 dB		−12 dB	
Communication system	PCL	mW	PCL	mW	PCL	mW
GSM900	PCL5	250	PCL8	63	PCL11	16
GSM1800	PCL0	125	PCL3	31	PCL6	8
UMTS[a]	–	∼250	–	∼63	–	∼16

[a] For devices of power class 3 (3GPP 2002).

audio signal turned on. The *B*-field decay from the phone surface was assessed by performing a 1D scan with a resolution of 1 mm perpendicular to the phone surface at one location on the front side of the phone. For all measurements, the microphone was turned off to prevent pick-up of sounds in the vicinity of the microphone.

Some measurements were performed using multiple RF power control levels (PCLs) (see table 3) to allow discrimination of the LF *B*-fields related to the communication system from other consumers. On the other hand, the influence of the power control in real networks and environments as well as the usage of discontinuous transmission were not assessed in this study.

The following configurations were measured for each DUT[4] in the GSM900, GSM1800, and UMTS bands:

- at highest PCL, i.e., 0 dB, with audio on: area scans (front, back, speaker);
- at PCL = −6 dB with audio off: area scan (front)[5];
- at PCLs = 0,−6,−12 dB:
  - audio off: z-scan, e.g., perpendicular to the phone surface (front, one location);
  - audio on: area scan (speaker), limited to 4 DUTs;
  - audio on: z-scan (speaker, one location), limited to 4 DUTs.

For *audio on* measurement configurations, a 1 kHz audio signal was transmitted from the AMMI to the CMU200 and then to the phone speaker via the radio interface. The audio signal was set at a normal speech level for GSM and UMTS, i.e., −16 dBm0 (ANSI 2007).

[4] Although the specifications of the MotorolaV1050 phone include UMTS, the connection in this band was very unstable and did not allow complete measurement; similar behavior was observed for GSM900 and GSM1800 at lower PCLs.

[5] For the slide and flip phones, only the surface of the phone on which the highest fields were measured, i.e., the bottom part close to the battery, was monitored at the lower power level.

Table 4. Uncertainty budget of the magnetic field measurements.

Error description	Unc. value (%)	Prob. dist.	Div.	Std. unc. (%)
Probe sensitivity				
Reference voltage at AMMI output	±3.0	N	1	±3.0
AMCC geometry	±0.4	R	$\sqrt{3}$	±0.2
AMCC current	±1.0	R	$\sqrt{3}$	±0.6
Probe positioning during calibration	±0.07	R	$\sqrt{3}$	±0.04
Noise contribution	±0.7	R	$\sqrt{3}$	±0.4
Probe system				
Repeatability/drift	±1.0	R	$\sqrt{3}$	±0.6
Linearity/dynamic range	±0.6	R	$\sqrt{3}$	±0.3
Probe angle	±2.3	R	$\sqrt{3}$	±1.3
Field disturbance	±0.2	R	$\sqrt{3}$	±0.1
Positioning				
Probe positioning	±1.9	R	$\sqrt{3}$	±1.1
DUT positioning	±8.3	R	$\sqrt{3}$	±4.8
Combined uncertainty				
Combined std. uncertainty				±6.0
Expanded std. uncertainty				±12.0

2.2.3. Uncertainty budget. The uncertainty budget of the measurement system was determined according to (ANSI 2007) (see table 4). The calibration of the probe was performed using a Helmholtz coil (AMCC, SPEAG, Switzerland).

2.2.4. Frequency range. The measurement setup characterization has shown that currents are induced in the coil sensor by vibrations when placed next to a permanent magnet, resulting in parasitic spectral components in the range 20–60 Hz with levels up to 1 μT, the same order of magnitude as the fields measured close to the phones' surfaces. As several permanent magnets can be found in mobile phones, e.g., at the speaker, to hold a pen, in the sliding mechanism, etc, the spectra were filtered to cut off frequencies below 60 Hz.

2.2.5. Detection limit. The response of the probe leads to a frequency-dependent detection limit. The sensitivity was assessed in the actual setup as well as with a mu-metal shielding (see figure 2). The detection limit was approximated by two linear functions (lower and higher than 80 Hz); any measurement data lower than this limit was considered as noise and was filtered out.

2.3. Numerical assessment

2.3.1. LF numerical solver. The LF currents induced in the human body by magnetic fields were analyzed with the Biot–Savart solver and the finite-element method implemented in SEMCAD X 14.8 (Chen *et al* 2013). Unlike typical finite-element methods, this implementation operates on rectilinear meshes, like the finite-difference time-domain method, allowing complex anatomical models to be easily rendered at various geometrical resolutions.

It is important to note that, when using the Biot–Savart quasi-static approximation, only the conductivity of the tissues needs to be specified. The *E*-field distribution of a simulation at a

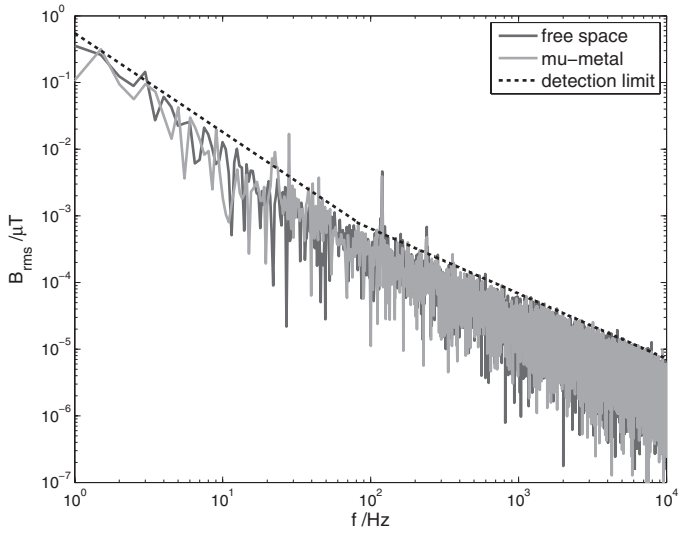

Figure 2. Detection limit of the measurement system with and without shielding from the ambient fields, mu-metal and free-space measurements, respectively.

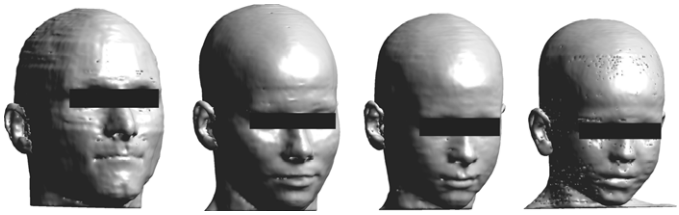

Figure 3. Anatomical head models from the Virtual Family: Duke, Ella, Billie, and Thelonious.

specific frequency f_0 can be scaled to another frequency (f/f_0), assuming that the conductivity contrasts between the tissues at f and f_0 are similar.

2.3.2. Anatomical heads. The numerical evaluations were conducted on the four anatomical heads from the Virtual Family (Christ *et al* 2010) (figure 3) developed and distributed by IT'IS (www.itis.ethz.ch/vip): Duke (34-year-old male), Ella (26-year-old female), Billie (11-year-old girl), and Thelonious (6-year-old boy).

For exposure to RF EMF, the dielectric properties of the tissues are typically assigned based on the 4-terms Cole–Cole fit of broadband measurement data presented by Gabriel *et al* (1996a, 1996b). However, for frequencies lower than 1 MHz, these values are associated with a large uncertainty.

The tissue properties used in this project are taken from the compilation available online at www.itis.ethz.ch/database (Hasgall *et al* 2011) and based on conductivity values from the literature review of Gabriel *et al* (2009) for frequencies up to 120 Hz (for more details, consult the documentation available online). For tissues for which no LF measurement was available, values from the 4-terms Cole–Cole fit were used.

The conductivity of skin at LF is problematic. For segmented models, in particular those of the Virtual Family, a homogeneous skin with a thickness of 2–4 mm is modeled. Reported LF conductivities of the skin often take only the outermost layer into consideration, the *stratum corneum*, which is about 0.1 mm thick and mainly made of dead cells (1×10^{-4} S m^{-1}). The uncertainty on this value is very high, particularly because it is highly dependent on the degree of moisture; reported values for wet skin in the LF range reach 2×10^{-3} S m^{-1} (Raicu *et al* 2000). These very low values of conductivity result in high and very localized induced fields, the volume of which is overestimated due to the homogeneous skin layer of the anatomical models. Additionally, the nerve endings do not reach the *stratum corneum* and the ICNIRP limits at low frequencies are based on nerve stimulation. Thus, a value of skin conductivity based on a weighted average of the components of its deeper layers (mainly muscles, fat, and blood), i.e., 1×10^{-1} S m^{-1}, as suggested by Dimbylow (2005), is more realistic and was used in this study.

2.3.3. Exposure scenarios. The numerical sources were placed on the left side[6] of the heads according to the procedure described in Kainz *et al* (2005). For the loop source that is used to model the fields from the communication system and the audio speaker, the uncertainty regarding the location of the maxima on the phone was taken into account by translating the sources by ± 10 mm in the plane of the phone, leading to a 3×3 exposure matrix.

2.4. Compliance with guidelines and standards

The exposure to non-ionizing radiation is regulated in most countries by guidelines developed either by the International Commission on Non-Ionizing Radiation Protection (ICNIRP) or the Institute of Electrical and Electronics Engineers (IEEE). The ICNIRP 1998 guidelines (ICNIRP 1998) cover frequencies from dc up to 300 GHz, whereas the 2010 guidelines (ICNIRP 2010) are specific for LF EMF (1 Hz–100 kHz). As both guidelines are presently in force, research groups interested in LF exposure usually compare compliance to both, as we also do here. The IEEE has published a safety standard for exposure to EMF at frequencies up to 3 kHz (IEEE 2002).

2.4.1. Basic restrictions. In ICNIRP (1998), EMF up to 10 MHz are limited by the maximum current density in the head and trunk (see table 5) to prevent effects on the nervous system, e.g., peripheral nerve stimulation and induction of phosphenes in the retina. The current density should be averaged over a cross-section of 1 cm^2, $\langle \mathbf{J} \rangle_{1\,\mathrm{cm}^2}$. In the LF guidelines (ICNIRP 2010), the internal electric field averaged over a small contiguous tissue volume of $2 \times 2 \times 2$ mm^3, $\langle \mathbf{E} \rangle_{8\,\mathrm{mm}^3}$, is used as the basic restriction (table 5). For each specific tissue, the guidelines specify that the 99th percentile value should be reported, an approach which has been criticized by several groups (De Santis *et al* 2012a, Laakso and Hirata 2012, Bakker *et al* 2012, Chen *et al* 2013). The influence of the definition of each tissue on the 99th percentile value is particularly relevant for localized exposure such as here. Finally, the IEEE (2002) standard defines basic restrictions in terms of the electric field averaged over a straight line segment of 5 mm length, $\langle \mathbf{E} \rangle_{5\,\mathrm{mm}}$ (table 6). The implementation of these averaging schemes in SEMCAD X is described in Chen *et al* (2013).

[6] The symmetry of the head and the exposure source allows us to assume similar results for exposure on the right side, as was already confirmed by Varsier *et al* (2008) and Gosselin *et al* (2011).

Table 5. ICNIRP basic restrictions (ICNIRP 1998, 2010) for general public exposure.

Frequency range	ICNIRP 1998 Current density mA m $^{-2}$ (rms) Head and trunk	ICNIRP 2010 Internal electric field V m^{-1} (rms) CNS head	ICNIRP 2010 Internal electric field V m^{-1} (rms) Head and body
Up to 1 Hz	8	–	–
1–4 Hz	$8/f$	$0.1/f$	0.4
4–10 Hz	2	$0.1/f$	0.4
10–25 Hz	2	0.01	0.4
25 Hz–1 kHz	2	$4 \times 10^{-4} f$	0.4
1–3 kHz	$f/500$	0.4	0.4
3–100 kHz	$f/500$	$1.35 \times 10^{-4} f$	$1.35 \times 10^{-4} f$
100 kHz–10 MHz	–	$1.35 \times 10^{-4} f$	$1.35 \times 10^{-4} f$

Table 6. IEEE C95.6-2002 basic restrictions (IEEE 2002) on the induced E-field, E_i, for general public exposure. $E_i = E_0$ for $f \leqslant f_e$; $E_i = E_0(f/f_e)$ for $f \geqslant f_e$.

Exposed tissue	f_e Hz	E_0 V m^{-1} (rms)
Brain	20	5.89×10^{-3}
Heart	167	0.943
Hands, wrists, feet, and ankles	3350	2.10
Other tissue	3350	0.701

2.4.2. Complex waveforms. The peak value of a time-domain signal cannot be directly compared to the safety limits, which are frequency dependent. A frequency-weighting technique for how to treat signals with frequency contents lower than 100 kHz (ICNIRP 2003) allows assessment independent of signal characteristics. This approach has been applied in various contexts, either including a frequency-dependent phase shift (Jokela *et al* 2004, Kännälä *et al* 2009), omitting it (Nadakuduti *et al* 2012), or comparing both (De Santis *et al* 2012b). We do not consider this phase shift here, as the rationale for doing so is unconvincing.

The ICNIRP guidance (ICNIRP 2003) suggests to use the basic restrictions to assess the conservativeness of the exposure, which is expressed in the original statement (ICNIRP 1998) in terms of current density. The time derivative of the magnetic flux density, $\mathrm{d}B/\mathrm{d}t$, can be derived from the current density $\mathrm{d}B/\mathrm{d}t = J/K_B$, where $K_B = 0.064$ A m^{-2} s T^{-1}. At each measurement point, the time-domain signal is first transformed to the frequency domain, where the normalized weighting function derived from the ICNIRP guidelines, based on B or $\mathrm{d}B/\mathrm{d}t$, is applied. The inverse Fourier transform (IFT) is then applied, and the weighted time-domain signal can be analyzed in terms of B or $\mathrm{d}B/\mathrm{d}t$ and compared to the limits used for the normalization of the weighting function. This treatment ensures that when there is constructive addition of the spectral components, it is taken into account in the compliance analysis. Thus, the ratio to the considered limit, or compliance factor, CF, can be expressed as

$$\mathrm{CF}_{\max}^{\mathrm{meas}} = \max \sqrt{\sum_{i=x,y,z} \left(\frac{\mathrm{d}}{\mathrm{d}t} \mathrm{IFT} \left(\frac{B_i^{\mathrm{meas}}(f)}{J_{\mathrm{lim}}(f)} K_B \right) \right)^2}, \tag{1}$$

for consideration of the basic restrictions, i.e., the limit in terms of J (or $\mathrm{d}B/\mathrm{d}t$).

The corner frequency used in the 2003 guidance (820 Hz) is based on the limit on occupational exposure. Here, we have chosen an approach consistent with the 1998 guidelines for general public exposure, using the current density values up to 100 kHz (see table 5).

2.4.3. Evaluation of numerical results. Simulations were performed at the frequency f_0—217 Hz for the communication system and 1 kHz for the audio signal—and the quantity of interest, $Q^{\mathrm{sim}}(f_0)$—which can be $\langle \mathbf{J} \rangle_{1\,\mathrm{cm}^2}$ (ICNIRP 1998), $\langle \mathbf{E} \rangle_{8\,\mathrm{mm}^3}$ (ICNIRP 2010), or $\langle \mathbf{E} \rangle_{5\,\mathrm{mm}}$ (IEEE 2002)—is extracted. To assess the exposure from the measured signals with a complex waveform, frequency scaling is applied. The results are normalized to the appropriate current by comparing the B-field from the measurement ($\mathbf{B}^{\mathrm{meas}}(f_0)\big|_{z=z_0}$) and the simulation ($\mathbf{B}^{\mathrm{sim}}(f_0)\big|_{z=z_0}$) in the plane $z = z_0$, and multiplied by the normalized spectral content ($B_z^{\mathrm{meas}}(f)/B_z^{\mathrm{meas}}(f_0)$):

$$Q^{\mathrm{sim}}(f) = Q^{\mathrm{sim}}(f_0) \times \frac{f}{f_0} \times \frac{\max(\mathbf{B}^{\mathrm{meas}}(f_0)|_{z=z_0})}{\max(\mathbf{B}^{\mathrm{sim}}(f_0)|_{z=z_0})} \times \frac{B_z^{\mathrm{meas}}(f)}{B_z^{\mathrm{meas}}(f_0)}. \tag{2}$$

Additional scaling to the conductivity should be performed for the current density, but since here the LF dielectric properties are used for most tissues (section 2.3.2), this is not necessary. The frequency-domain signal is weighted with the frequency-dependent limits, $\mathrm{Lim}(f)$, and transformed back to the time domain, where the maximum is extracted. The compliance factor is, thus, given by

$$CF_{\max}^{\mathrm{sim}} = \max\left(\mathrm{IFT}\left(\frac{Q^{\mathrm{sim}}(f)}{\mathrm{Lim}(f)}\right)\right). \tag{3}$$

3. Validation of experimental setup

The experimental setup was validated by measuring the magnetic fields of a calibrated telephone magnetic field simulator (TMFS, SPEAG, Switzerland) and a thin wire fed by a sinusoidal source. The peak magnetic field reading 10 mm above the TMFS deviated <3% from the target value. The maximum value of magnetic field measured with a resolution of 0.7 mm in a plane 1 mm above the thin wire was 3.45 μT, deviating <3% from the analytically determined target value of 3.42 μT. Both deviations are well within the total expanded measurement uncertainty of the system of 7.3% (table 4) when the uncertainty due to the phone positioning is disregarded.

4. Experimental assessment

4.1. Frequency content

Figure 4 shows the frequency content for all phones at frequencies up to 500 Hz. As expected for the GSM communication system, fields at 217 Hz and harmonics are measured with all phones at 900 and 1800 MHz. Although the experimental setup did not allow measurements lower than 60 Hz, the 8.3 Hz component of the GSM communication system is seen by the presence of its harmonics in figures 4(a) and (b).

For UMTS, the fields are in general much smaller than for GSM—note that the B-field axis in figure 4(c) is a factor of 100 smaller than for figures 4(a) and (b). Further, no frequency component is systematically much larger than the others, e.g., the power control performed at a frequency of 1500 Hz does not draw current bursts from the battery. A more detailed analysis showed that, for all phones, a 100 Hz component can be detected, most probably due to the time frame of 10 ms used in UMTS.

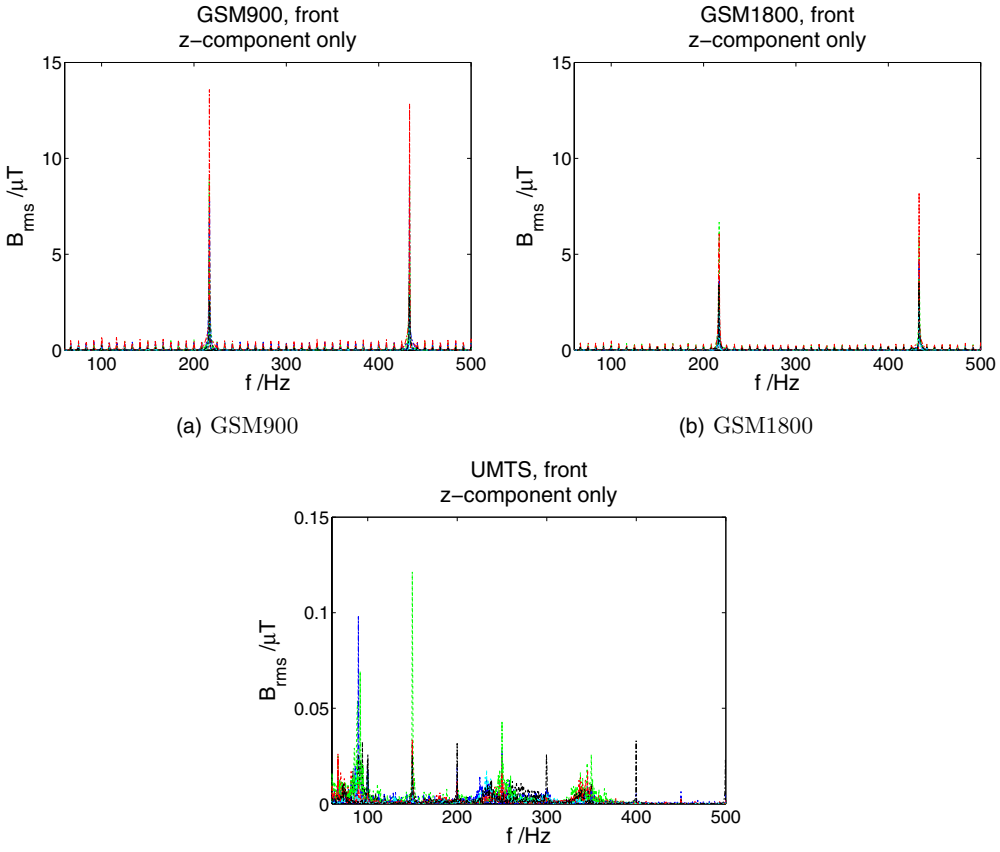

Figure 4. Superposition of the frequency spectrum from all phones up to 500 Hz. The maximum value of the *B*-field axis is 15 μT for GSM and 0.15 μT for UMTS. (a) GSM900. (b) GSM1800. (c) UMTS.

4.2. Spatial distribution

The spatial distribution of the fields—217 Hz for GSM and 100 Hz for UMTS—was extracted for all phones, and the maximum was always found near the feedpoint of the battery: e.g., figure 5 shows the *B*-field spatial distribution of the SamsungGT-I9001 phone. At each measurement point, the field at the target frequency is extracted from the frequency-domain signal by integrating the *B*-field over a 3 dB bandwidth. Equivalent high-resolution scanning was performed around the speaker area with the 1 kHz signal, shown in figure 6. The speaker pattern is consistent with a current loop and is independent of the communication system.

4.3. Decay with separation from the DUT

The decay with the separation from the surface of each DUT, investigated by performing a scan along a 3 cm line perpendicular to the DUT surface at the location of the maximum, was performed at three PCLs. Figure 7 shows the decay of the *B*-field close to the battery feedpoint

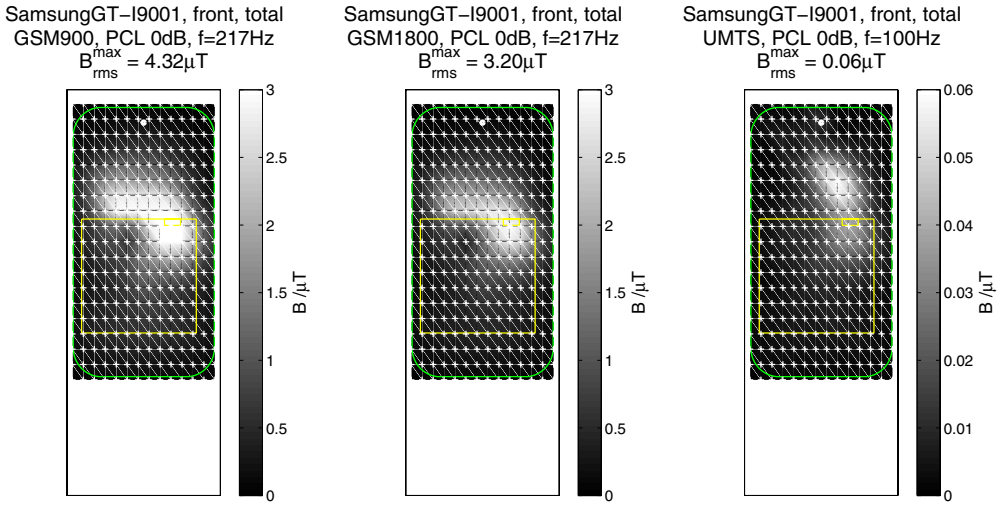

(a) GSM900 (b) GSM1800 (c) UMTS

Figure 5. *B*-field spatial distribution on the front of the SamsungGT-I9001 phone at maximum PCL for (a) GSM900 (217 Hz), (b) GSM1800 (217 Hz), and (c) UMTS (100 Hz); the outline of the phone and the battery are shown; the *B*-field scale for GSM is up to 6 μT and for UMTS up to 0.4 μT.

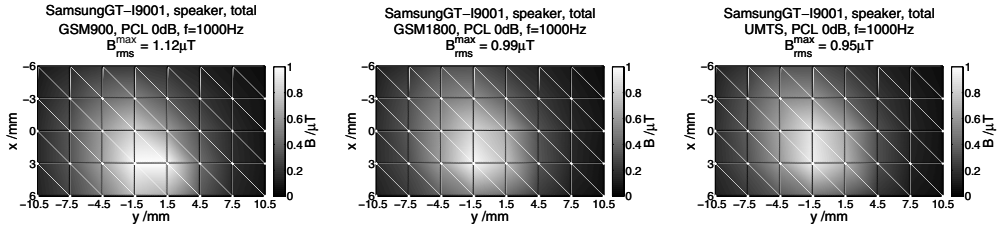

(a) GSM900 (b) GSM1800 (c) UMTS

Figure 6. *B*-field spatial distribution at 1 kHz around the speaker of the SamsungGT-I9001 phone with audio ON for (a) GSM900, (b) GSM1800, and (c) UMTS.

(217 Hz for GSM[7]) and figure 8 shows the decay near the speaker (1 kHz). The results confirm that the 217 Hz component in GSM mode is directly related to the current drawn from battery as a consequence of the radio communication, yet the 1 kHz signal at the speaker is directly related to the audio signal.

4.4. Compliance with the ICNIRP reference levels

The compliance of complex waveforms with the ICNIRP reference levels is assessed as described in section 2.4.2, and the compliance factor (in terms of dB/dt) is calculated according to (1). Table 7 reports the maximum extracted ratio for each phone and communication system. The maximum ratios of measured waveform to the ICNIRP limits for GSM900 are higher than for GSM1800, which is consistent with the higher output power used. For all phones,

[7] The decay in UMTS is not shown, as the level is very low and mainly consists of noise.

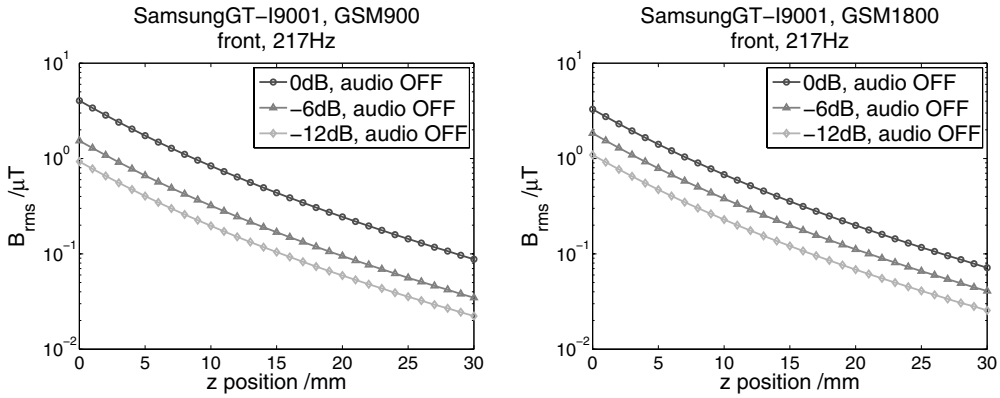

(a) GSM900 (b) GSM1800

Figure 7. *B*-field along a line perpendicular to the surface of the SamsungGT-I9001 phone at 217 Hz for (a) GSM900 and (b) GSM1800.

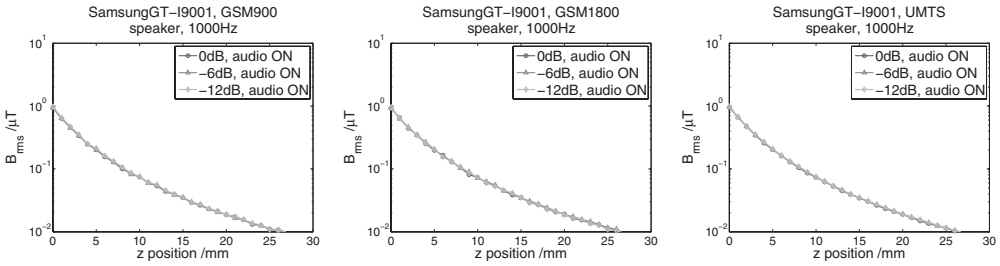

(a) GSM900 (b) GSM1800 (c) UMTS

Figure 8. *B*-field along a line perpendicular to the surface of the SamsungGT-I9001 phone at 1 kHz close to the speaker with audio ON for (a) GSM900, (b) GSM1800, and (c) UMTS.

Table 7. Compliance factor in terms of the ICNIRP limit on dB/dt with all frequencies from the communication systems under consideration.

	GSM900	GSM1800	UMTS
HTCdiam100	4.33	2.95	0.23
HTCtopa100	4.32	1.99	0.23
LG	2.39	1.58	0.24
MotorolaV1050	1.20	1.17	
Nokia6120	2.75	2.10	0.37
SamsungGT-I9001	2.24	1.65	0.15
SonyEricssonW760i	1.15	1.01	0.52
SonyEricssonW910	5.63	3.81	0.27
iPhone3 g	1.25	1.06	0.73
iPhone4	1.44	1.51	0.59

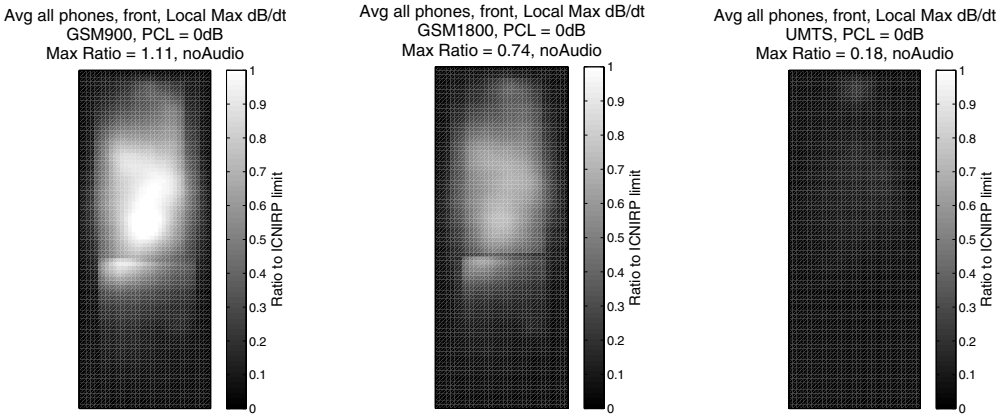

(a) GSM900 (b) GSM1800 (c) UMTS

Figure 9. Envelopes of the point-wise maximum ratio of exposure to the ICNIRP 1998 limits from all phones at the maximum PCL, excluding the contribution from the audio signal, for (a) GSM900, (b) GSM1800, and (c) UMTS.

the exposure in UMTS is lower than in GSM by at least 25%, and up to a factor of 19 when compared to GSM900.

4.5. Worst-case equivalent sources

To derive the envelope of the exposure (for GSM900, GSM1800, and UMTS), the compliance factor in terms of $\mathrm{d}B/\mathrm{d}t$ was extracted (1) from the spatial distributions on the front side of every phone. The speaker point of each phone was superposed, and, for each location, the maximum value from all phones is reported.

Figure 9 shows the envelope of the exposure from GSM900, GSM1800, and UMTS from all phones at the maximum PCL. These results are used for the development of the numerical source (section 5).

5. Development of numerical sources

As reported in section 4.2, the maximum LF fields are typically located close to the feedpoint of the phone battery, thus distributions are strongly phone-design dependent. The worst-case equivalent source should not be representative of any single phone, but rather a conservative estimate for all phones. We have, thus, designed a numerical source from an array of loops that produces a rather uniform B-field enveloping the measured distributions. The loops are fed with ideal current sources. The distance of this array from the head has been set such that the decay of the fields corresponds to the measurements performed in GSM mode, since measurements made in UMTS mode are too close to the detection limit. The loops' currents have been set such that the maximum B-field at 4 mm distance matches the maximum measured field in this plane for the individual phones.

In the LF range, the induced current density is the quantity that limits the exposure, and maximum coupling is obtained with the B-field perpendicular to the surface of the body. Thus,

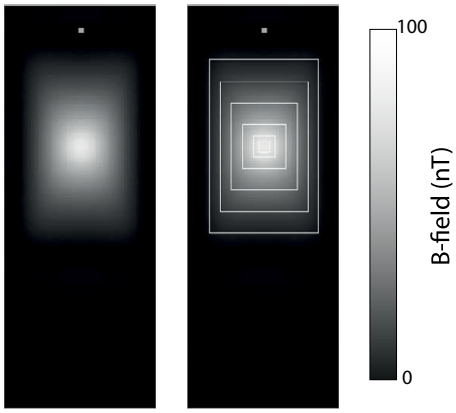

Figure 10. B_z^{rms} generated by the array of rectangular loops (left) and superposed on the loops in white (right); the same plotting area is used as in figure 9.

the numerical source has been developed with the focus mainly on the fields perpendicular to the phone's surface, i.e., along the z-axis.

Figure 10 shows the B_z-field from the numerical source. The effective distance of the loops was found to be 11 mm.

The same procedure was applied to the 1 kHz fields from the speaker, where the loop radius was set to 4 mm; from the comparison to the measurements, a distance of 3 mm was found for the location below the phone surface.

6. Numerical assessment

The compliance factor calculated from (3) with respect to the corresponding limit from ICNIRP or IEEE was evaluated for all averaging schemes, phones, communication systems, and anatomical heads. Figure 11(a) shows that the ratio of the surface-averaged current density does not exceed 40% of the ICNIRP limit for GSM900. The spread of the values for the various positions of the numerical source is larger than the difference between adults and children. However, the spread of the compliance factors for any particular phone for the children is larger than for the adults, which is expected, since a translation of 10 mm is larger in proportion to the head size.

At GSM1800 (figure 11(b)), the distribution is similar although all the values are slightly smaller than for GSM900. For UMTS (figure 11(c)) the maximum value is lower than for GSM by about two orders of magnitude. Only the results of GSM900 are used to compare the remaining parameters of the analysis.

Figure 12 shows that the application of the current density limits from the ICNIRP 1998 guidelines to all tissues (figure 12(a)) or to the central nervous system (CNS) tissues only (figure 12(b)) does not lead to significant differences for the type of exposure presented here. The spread of the line-averaged E-field values (figure 13, IEEE) from various positions is larger for CNS tissues than for all tissues. Indeed, the structure of the tissues around the cheek area, where the exposure is maximum, is rather smooth, such that small translations of the loop array do not lead to very different exposure patterns; the structures of the CNS, however, are more complex, and relatively small translations can lead to significantly different exposures. Also, as the CNS tissues do not include peripheral tissues, smaller E-field-to-limit ratios are

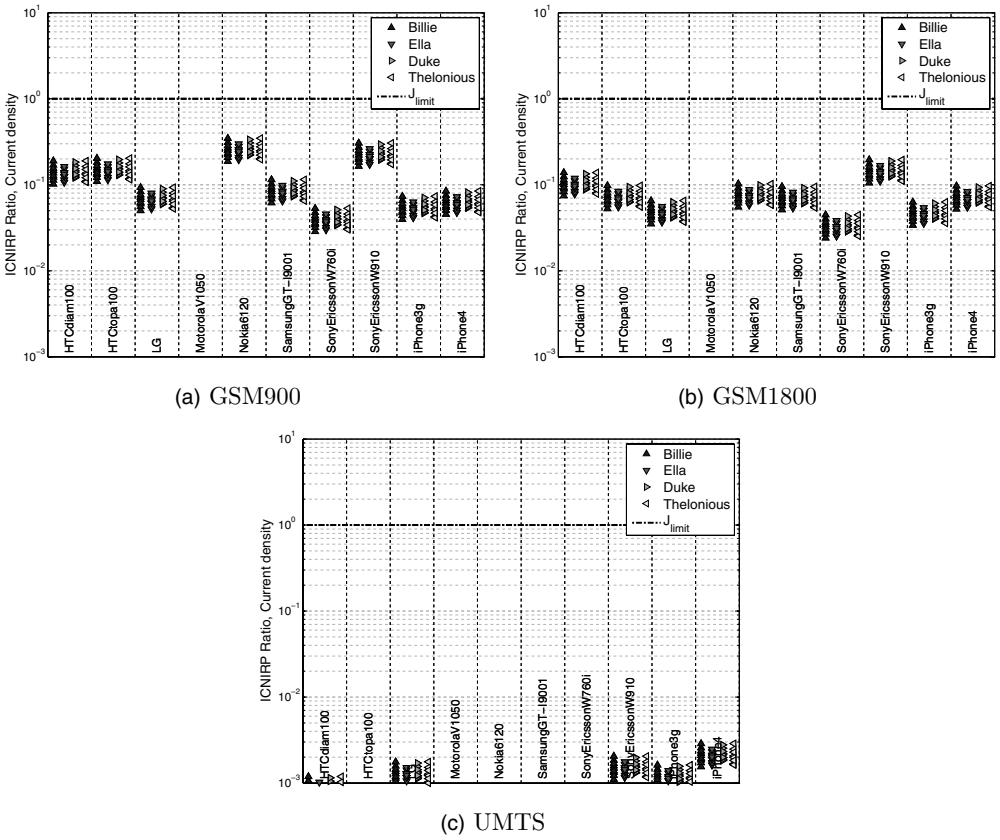

(a) GSM900 (b) GSM1800

(c) UMTS

Figure 11. Ratio of the surface-averaged current density to the ICNIRP 1998 limits for all tissues, in (a) GSM900, (b) GSM1800, and (c) UMTS.

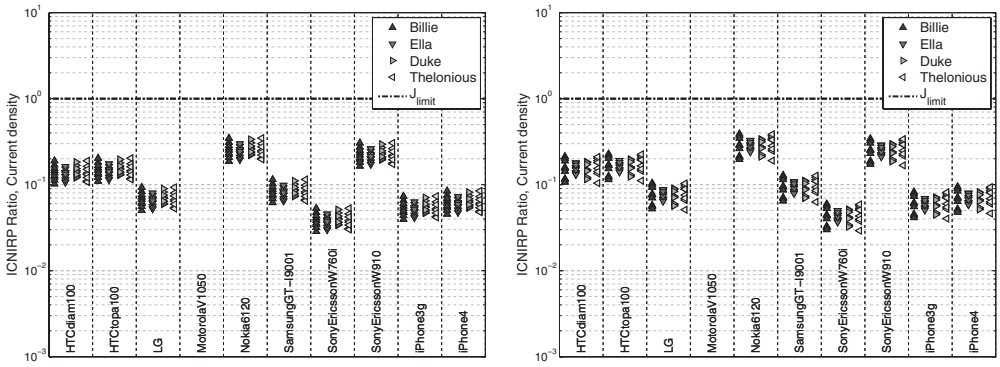

(a) J_{surf}, all tissues (b) J_{surf}, CNS tissues

Figure 12. Ratio of the surface-averaged current density to the ICNIRP 1998 limits in GSM900 for (a) all tissues and (b) CNS tissues.

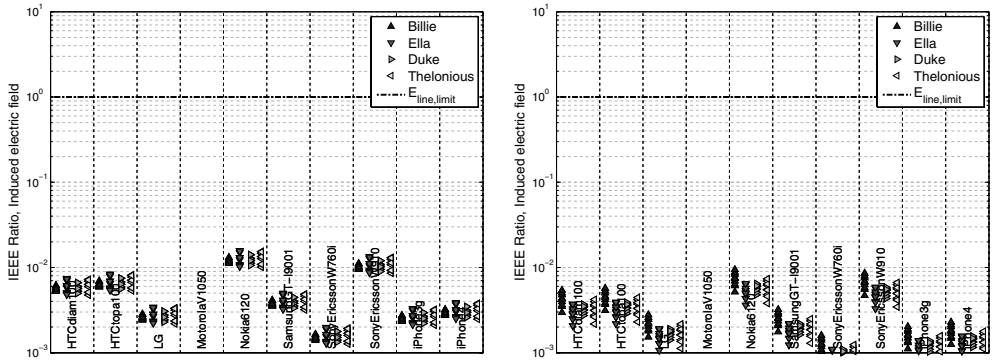

(a) E_{line}, all tissues (b) E_{line}, CNS tissues

Figure 13. Ratio of the line-averaged induced electric field to the IEEE limits in GSM900 for (a) all tissues and (b) CNS tissues.

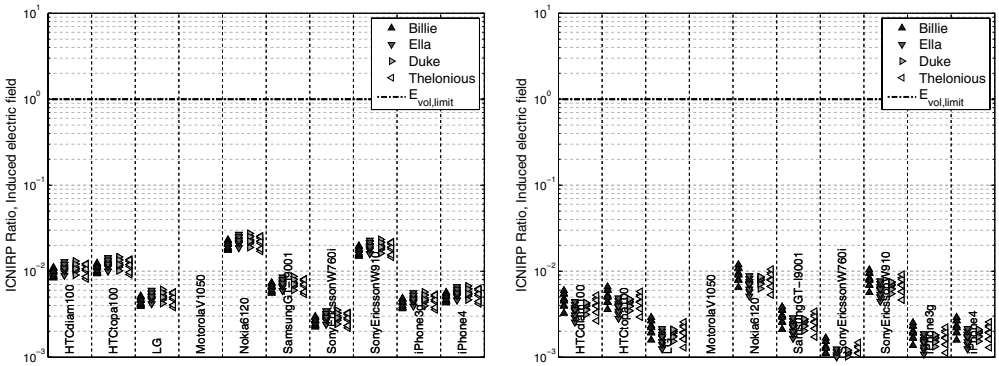

(a) E_{vol}, all tissues (b) E_{vol}, CNS tissues

Figure 14. Ratio of the volume-averaged induced electric field to the ICNIRP 2010 limits in GSM900 for (a) all tissues and (b) CNS tissues.

found. Similar results were obtained for the volume-averaged induced *E*-field (ICNIRP 2010, figure 14).

Among the three quantities and averaging schemes used for compliance assessment, the current density from the ICNIRP 1998 guidelines is the most restrictive, by roughly one order of magnitude.

Finally, the exposure was assessed for an audio signal at 1 kHz. Figure 15 shows the induced current density (ICNIRP 1998), and figure 16 shows the induced fields averaged along a line according to the IEEE standard. The ear is a more complex structure than the cheek and is located very close to the loop, such that small translations can lead to large differences in the peak exposure: a larger variation with the position of the loop is observed with this more localized exposure when all the tissues are considered than for CNS tissues only.

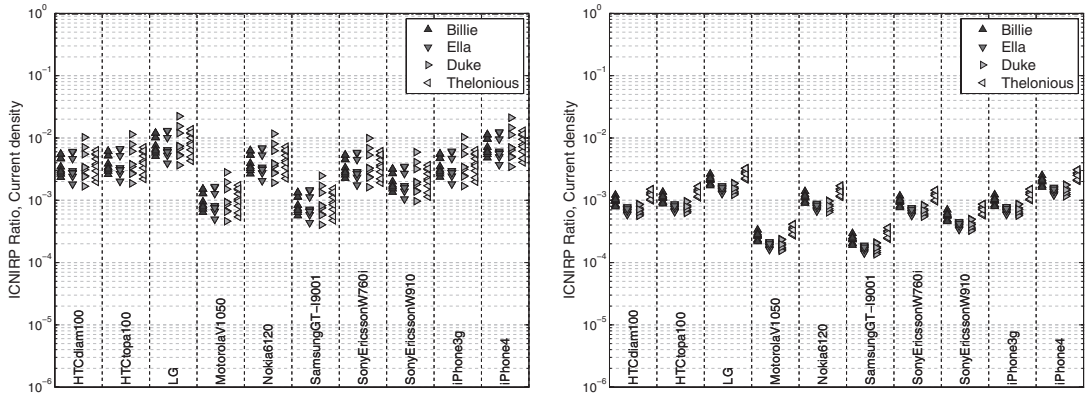

(a) J_{surf}, all tissues (b) J_{surf}, CNS tissues

Figure 15. Ratio of the surface-averaged current density to the ICNIRP 1998 limits for the audio signal at 1 kHz for (a) all tissues and (b) CNS tissues.

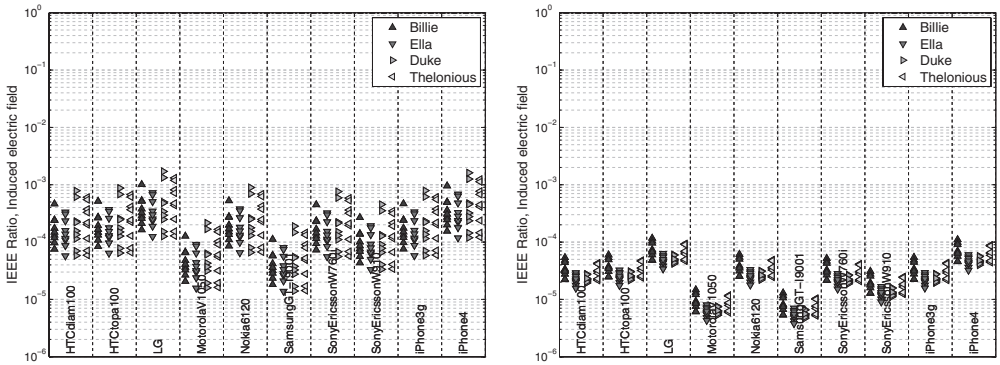

(a) E_{line}, all tissues (b) E_{line}, CNS tissues

Figure 16. Ratio of the line-averaged induced electric field to the IEEE limits for the audio signal at 1 kHz for (a) all tissues and (b) CNS tissues.

7. Discussion and conclusions

From the assessment of compliance with the ICNIRP guidelines for the complex waveforms generated, we have found that the reference levels were exceeded by up to a factor of 5.6 in the measurement plane, i.e., 4 mm from the phone surface. Considering the measured decay along the axis perpendicular to the phone surface, we found that the compliance factor reduces to a factor of 3 at the distance of the gray matter from the phone surface (12.6 mm for Billie). For the worst-case phone, compliance with the reference levels would be achieved only at a distance of 18 mm. The LF fields generated by mobile phone battery currents are, thus, not compliant with the ICNIRP reference levels for normal use, i.e., at the head. However, the assessment in terms of basic restrictions related to the induced fields or currents has shown that the exposure reaches at most 40% of the limits for ICNIRP 1998, but one order of magnitude lower for ICNIRP 2010 and IEEE. In addition, it is interesting to note that the contribution

from the audio signal at a normal speech level, i.e., −16 dBm0, is the same order of magnitude as the fields induced by the current bursts generated from the implementation of the global system for mobile (GSM) communication system.

The current-induced *B*-field generated from the communication system via the UMTS are two orders of magnitude lower than via GSM, which disproves the hypothesis that higher low-frequency (LF) fields are generated with the UMTS due to the high current consumption of the complex processing circuitry. This finding provides useful information regarding LF fields generated during UMTS use, and, together with the knowledge that RF exposure from the UMTS is two orders of magnitude lower than from GSM, we may now state that there is an overall reduction in the average exposure when this communication system is used.

Open questions remain, e.g., related to the use of UMTS-TDD, which could lead to different results. We did not consider UMTS-TDD in this project, as the devices used do not support this technology. In addition, TDD is intended mainly for data transfer, where the exposure at the head is not a main concern other than for voice over Internet protocols (VoIP). Further studies should include UMTS-TDD in the context of VoIP as well as very recent communications technologies such as TD-SCDMA, LTE for VoIP, and EV-DO (an extension of CDMA2000) for VoIP.

Finally, the power control scheme in GSM based on hard handovers could lead to additional LF components in the spectrum, but these would be dependent on the network and the movements of the user holding the mobile device. These components are expected to carry much less energy than those related to the time-frame structure of the communication system.

Acknowledgments

This research project was financed by the FSM (Research Foundation Mobile Communication). Marie-Christine Gosselin is a NSERC (Natural Sciences and Engineering Research Council of Canada) grant holder.

References

3GPP 1999 Digital cellular telecommunications system (phase 2+): radio transmission and reception 3GPP TS 05.05 version 8.6.0, release 1999

3GPP 2002 UE Radio transmission and reception (FDD) *3GPP TS 25.101* version 5.2.2, release 5

Andersen J B, Mogensen P E and Pedersen G F 2010 Power variations of wireless communication systems *Bioelectromagnetics* **31** 302–10 (www.ncbi.nlm.nih.gov/ pubmed/20112260)

Andersen J B and Pedersen G F 1997 *Radiat. Prot. Dosim.* **72** 249–57

ANSI 2007 American National Standards methods of measurement of compatibility between wireless communications devices and hearing aids ANSI C63.19-2007 (New York The American National Standards Institute) pp 1–145

Bakker J F, Paulides M M, Neufeld E, Christ A, Chen X L, Kuster N and van Rhoon G C 2012 Children and adults exposed to low-frequency magnetic fields at the ICNIRP reference levels: theoretical assessment of the induced electric fields *Phys. Med. Biol.* **57** 1815–29

Chen X L, Benkler S, Chavannes N, De Santis V, Bakker J, van Rhoon G, Mosig J and Kuster N 2013 Analysis of human brain exposure to low-frequency magnetic fields: a numerical assessment of spatially averaged electric fields and exposure limits *Bioelectromagnetics* **34** 375–84

Christ A *et al* 2010 The virtual family – development of surface-based anatomical models of two adults and two children for dosimetric simulations *Phys. Med. Biol.* **55** N23–38

De Santis V, Douglas M, Nadakuduti J, Benkler S and Kuster N 2012b Exposure evaluation of therapeutic magnetic field mats *Technical Report* BAG 11.002460/434.0000/-99 (Zurich: ITIS Foundation)

De Santis V, Douglas M, Kuster N and Chen X L 2012a *EMC EUROPE'12: Int. Symp. on Electromagnetic Compatibility* pp 1–4

Dimbylow P 2005 Development of the female voxel phantom, NAOMI, and its application to calculations of induced current densities and electric fields from applied low frequency magnetic and electric fields *Phys. Med. Biol.* **50** 1047–70

Gabriel C, Peyman A and Grant E 2009 Electrical conductivity of tissue at frequencies below 1 MHz *Phys. Med. Biol.* **54** 4863–78

Gabriel S, Lau R W and Gabriel C 1996a The dielectric properties of biological tissues: II. Measurements in the frequency range 10 Hz to 20 GHz *Phys. Med. Biol.* **41** 2251–69

Gabriel S, Lau R W and Gabriel C 1996b The dielectric properties of biological tissues: III. Parametric models for the dielectric spectrum of tissues *Phys. Med. Biol.* **41** 2271–93

Gosselin M C, Kühn S, Crespo-Valero P, Cherubini E, Zefferer M, Christ A and Kuster N 2011 Estimation of head tissue-specific exposure from mobile phones based on measurements in the homogeneous SAM head *Bioelectromagnetics* **32** 493–505

Hasgall P, Neufeld E, Gosselin M C, Klingenböck A and Kuster N 2011 Thermal and electromagnetic parameters of biological tissues *ITIS database* (Reston, VA: Integrated Taxonomic Information System) available at www.itis.ethz.ch/database

ICNIRP 1998 Guidelines for limiting exposure to time-varying electric, magnetic, and electromagnetic fields (up to 300 GHz) *Health Phys.* **74** 494–522

ICNIRP 2003 Guidance on determining compliance of exposure to pulsed and complex non-sinusoidal waveforms below 100 kHz with ICNIRP guidelines *Health Phys.* **84** 383–7

ICNIRP 2010 Guidelines for limiting exposure to time-varying electric and magnetic fields (1 Hz to 100 kHz) *Health Phys.* **99** 818–36

IEEE 2002 IEEE Standard for Safety Levels with Respect to Human Exposure to Electromagnetic Fields 0–3 kHz *IEEE Std* C95.6-2002 (New York: IEEE)

Ilvonen S and Sarvas J 2007 Magnetic-field-induced ELF currents in a human body by the use of a GSM phone *IEEE Trans. Electromagn. Compat.* **49** 294–301

Ilvonen S, Sihvonen A P, Kärkkäinen K and Sarvas J 2005 Numerical assessment of induced ELF currents in the human head due to the battery current of a digital mobile phone *Bioelectromagnetics* **26** 648–56

Jokela K, Puranen L and Sihvonen A P 2004 Assessment of the magnetic field exposure due to the battery current of digital mobile phones *Health Phys.* **86** 56–66

Kainz W, Christ A, Kellom T, Seidman S, Nikoloski N, Beard B and Kuster N 2005 Dosimetric comparison of the specific anthropomorphic mannequin (SAM) to 14 anatomical head models using a novel definition for the mobile phone positioning *Phys. Med. Biol.* **50** 3423–45

Kännälä S, Toivo T, Alanko T and Jokela K 2009 Occupational exposure measurements of static and pulsed gradient magnetic fields in the vicinity of MRI scanners *Phys. Med. Biol.* **54** 2243–57

Kuehn S and Kuster N 2013 Field evaluation of the human exposure from multiband, multisystem mobile phones *IEEE Trans. Electromagn. Compat.* **55** 275–87

Laakso I and Hirata A 2012 Reducing the staircasing error in computational dosimetry of low-frequency electromagnetic fields *Phys. Med. Biol.* **57** N25–34 www.ncbi.nlm.nih.gov/pubmed/22290579

Nadakuduti J, Douglas M, Capstick M, Kühn S and Kuster N 2012 Application of an induced field sensor for assessment of electromagnetic exposure from compact fluorescent lamps *Bioelectromagnetics* **33** 166–75

Pedersen G F and Andersen J B 1999 RF and ELF exposures from cellular phone handsets: TDMA and CDMA systems *Radiat. Prot. Dosim.* **83** 131–8 http://rpd.oxfordjournals.org/ content/83/1-2/131.short

Perentos N, Iskra S, McKenzie R J and Cosic I 2007 Characterization of pulsed ELF magnetic fields generated by GSM mobile phone handsets *IFMBE Proc.* **14** 2706–9

Perentos N, Iskra S, McKenzie R J and Cosic I 2008 Simulation of pulsed ELF magnetic fields generated by GSM mobile phone handsets for human electromagnetic bioeffects research *Australas. Phys. Eng. Sci. Med.* **31** 235–42

Raicu V, Kitagawa N and Irimajiri A 2000 A quantitative approach to the dielectric properties of the skin *Phys. Med. Biol.* **45** L1–4

Tuor M, Ebert S, Schuderer J and Kuster N 2005 Assessment of ELF exposure from GSM handsets and development of an optimized RF/ELF exposure setup for studies of human volunteers *Technical Report* BAG 2.23.02.-18/02.001778 (Zurich: ITIS Foundation)

Varsier N, Wake K, Taki M, Watanabe S, Takebayashi T, Yamaguchi N and Kikuchi Y 2008 SAR characterization inside intracranial tumors for case-control epidemiological studies on cellular phones and RF exposure *Ann. Telecommun.* **63** 65–78

Wiart J, Dale C, Bosisio A V and Le Cornec A 2000 Analysis of the influence of the power control and discontinuous transmission on RF exposure with GSM mobile phones *IEEE Trans. Electromagn. Compat.* **42** 376–85